Structural, Electrical, Magnetic and Optical Properties of BaTi1-x(Ni1/2Nb1/2)xO3 Ceramics

sheng li
East China Normal University
yuanyuan zhang (yyzhang@ee.ecnu.edu.cn)
East China Normal University https://orcid.org/0000-0002-3765-7298
Lisa Zhou
East China Normal University
Qingqing Liu
East China Normal University
Jing Yang
East China Normal University
Wei Bai
East China Normal University
Xiaodong Tang
East China Normal University

Research Article

Keywords: doping, Ferroelectric properties, Magnetic properties, BaTiO3

Posted Date: March 15th, 2021

DOI: https://doi.org/10.21203/rs.3.rs-291189/v1

Abstract

In this work, we have investigated the structural, electrical, magnetic and optical properties of Ni-Nb co-doped $BaTiO_3$ ceramics. The compositions of $BaTi_{1-x}(Ni_{1/2}Nb_{1/2})_xO_3$ were prepared through conventional solid-state reaction method. All the samples exhibit a gradual phase transition behavior from the tetragonal to a cubic structure with the increase of Ni-Nb co-doping concentration. The temperature dependence of the dielectric constant reveals that the transition temperature gradually decreased with an increase in Ni^{2+} and Nb^{5+} concentrations. The ferroelectric studies show these doping samples have relatively full ferroelectric hysteresis loops at room temperature, but exhibit a decreasing ferroelectric property with the increasing level of doping. The magnetic measurement suggests that these samples have ferromagnetic ordering at room temperature with an increase in the Ni-Nb doping. Moreover, band gaps of these samples are obviously reduced through the strategy of co-doping.

1. Introduction

Multiferroic materials have rich physical properties and wide application prospects, such as in the fields of multi-state data storage, sensor devices and solar photovoltaic[1–4]. Multiferroic materials have been defined as a type of materials that possess two or more of ferromagnetism, ferroelectricity and ferroelasticity. Recently, much attention is paid to ABO_3 perovskites due to their unique structure and multiferroic properties. In perovskite materials, ferroelectricity is caused by the off-center displacement of the transition metal ion with the d^0 configuration located in the center of the octahedron[5]. Almost the known ferroelectric perovskites contain transition metal ions with the d^0 configuration, such as Ti^{4+}. On the contrary, the existence of electrons in the d orbital is a necessary condition for the formation of the magnetism[6]. Therefore, this ferroelectric behavior and ferromagnetic behavior tend to exclude one another in ABO_3 perovskites. One possible way to acquired multiferroic is to make the configuration d^0 and d^n ions coexist[7]. Thus, in order to obtain single-phase multiferroic materials, doping ferroelectric materials is currently a common method.

ABO_3 ferroelectrics have been extensively studied due to their diverse properties that can be regulated by suitable changes in the structure and chemistry, which means it has potential to be multiferroic by purposeful regulation. $BaTiO_3$ (BTO) is a typical ABO_3 perovskite-type material, which can be used in many applications because it can maintain large ferroelectricity with high ferroelectric Curie temperature (T_C)[8]. As the temperature decreases, the crystalline structure of BTO changes from hexagonal ($P_{63/mmc}$) phase to cubic (P_{m3m}) phase, to tetragonal (P_{4mm}) phase, to orthorhombic (A_{mm2}) phase and finally to rhombohedral (R_{3m}) phase orderly. In addition to temperature, the doping also affects the crystalline structure of the BTO ceramics, which can modulate the physical properties of the material[9, 10]. So far, many studies have only focused on electric properties of BTO-based materials, but their coexistence of magnetic and ferroelectricity is rarely considered. In recent years, Hiroyuki *et al*. predicted that Mn-doped BTO have multiferroic based on total energy calculations[11]. Partial substitution of the Ti-site ions by transition metal ions possessing the d^n configuration have simultaneously ferromagnetism and ferroelectricity at room temperature, which makes it a promising single-phase multiferroic material at room temperature[12–15]. In the existing research, past attempts to induce ferromagnetism of the BTO ceramic by the single-doping with the d^n configuration which do not favor ferroelectricity have resulted in a rapid decrease of ferroelectricity[6, 16]. The reason is that even the dopant of a small amount of transition metal ions in BTO will also cause its crystalline structure to quickly degrade from the ferroelectric tetragonal phase to the paraelectric hexagonal phase, thereby dramatically reducing the ferroelectricity[13]. Single-doping in BTO can easily form a hexagonal phase, so a co-doping strategy should be adopted to avoid the generation of hexagonal phase[13, 17]. Recently, some researchers have discovered that the co-doping of transition metal ions and Nb^{5+} ion can transform perovskite-type materials from tetragonal to cubic phases[14]. This adjustment of the crystalline structure can significantly slow down the reduction of its ferroelectric properties. Additionally, the introduction of transition metal ions have an effect on the band gap of the BTO ceramic, which makes it provide a promising prospect in the solar photovoltaic industry[17].

In this paper, we use conventional solid-state sintering methods to synthesize $BaTi_{1-x}(Ni_{1/2}Nb_{1/2})_xO_3$ (BTNNO) ceramics for structural, electrical, magnetic and optical properties study. With the increasing dopant concentration, the crystalline structure of samples transforms from tetragonal to cubic, accompanied by a decrease in ferroelectricity slowly. The temperature dependent dielectric properties are measured in the frequency range from 1 kHz to 1 MHz. The magnetic properties have been investigated in detail. In addition, the replacement of the B-site ion also adjusts the optical band gap, so the influence of dopant concentration on the band gap will also be discussed.

2. Experimental

The solid solutions $BaTi_{1-x}(Ni_{1/2}Nb_{1/2})_xO_3$ (x = 0, 0.02, 0.04, 0.06, 0.08 and 0.1) were synthesized by a solid-state reaction using $BaCO_3$ (99%), TiO_2 (98%), Nb_2O_5 (99.5%), and Ni_2O_3 (99%) as raw materials. These raw materials were weighted according to their stoichiometric ratios. The mixed powders were ball milled with agate balls in deionized water for 8 h at the speed of 400 r/min. Next, the slurry was dried in an oven at 70 ℃ and then calcined at 1150 ℃ or 2 h. After calcination, the mixtures were is ground into powders in order to passing through the 40-mesh sieve and then balls milled again for another 8 h. After dried out, the powders were mixed with 8 wt% PVA and pressed into disks with the diameter of 12 mm and 2 mm thick. During calcination, the temperature is maintained at 800 ℃ for 2 h and then heated to 1350 ℃ for 2 h at the heating rate of 5 k/min. Finally, silver electrodes covered both sides of the sample for further electrical measurements.

The X-ray diffraction (XRD, PANalytical EMPTREAN S3) characterizes the crystalline structure of ceramic samples for the angular range of 2θ from 20^o to 80^o. Dielectric constant were measured using a precision LCR meter (Agilent E4980A) mounted on PPMS-9T over the frequency range of 20 Hz-1 MHz within the temperature range of 10–400 K. The ferroelectric loops were tested at a frequency of 100 Hz. The magnetic properties were measured by a Superconducting Quantum Interference Device (SQUID, Quantum Design, USA). The transmittance spectra were measured by a double beam ultraviolet-infrared spectrophotometer (Perkin Elmer UV/VIS Lambda 950) at the photon energy of 0.5–6.5 eV (2650 – 190 nm) with 2 nm intervals at room temperature.

3. Results And Discussion

As illustrated in Fig. 1(a), we observe the structural changes of Ni-Nb co-doped BTO ceramics under different doping concentration through X-ray diffraction pattern. The pure $BaTiO_3$ and all the doped samples possess pure perovskite structure without impurity phases, manifesting that Nb^{5+} and Ni^{2+} dissolved in $BaTiO_3$ lattice to form solid solutions due to the comparable ionic radii[18, 19]. The solubility of doped ions in the $BaTiO_3$ system mainly depends on the radius of the doped ions. The radii of Ni^{2+} (0.690Å) and Nb^{5+} (0.640Å) are close to the ionic radius of Ti^{4+} (0.605Å) ions, thus helping Ni^{2+} to replace Ti^{4+} ions[20, 21]. Furthermore, as can be seen clearly in the 2θ range of 44.5^{o}-46^{o} in Fig. 1(b), two peaks of (200) and (002) gradually combine a single peak with the increasing dopant concentration, meaning structural transition from tetragonal to cubic phase. Therefore, it can be suggested that tetragonal and cubic phases coexist in the doping composition range of $0.02 < x < 0.1$. It is evident that the substitution of Ni-Nb pairs for Ti will lead to the formation of cubic phase in Ni-Nb co-doped BTO ceramics.

Relationship between dielectric constant and temperature of the BTNNO samples at 10 K-400 K at different frequencies over the range of 1 kHz to 1 MHz is displayed in Fig. 2(a-e). With temperature decreasing, T_C marks the transition of distinct phase from cubic and tetragonal phase. These transitions show sharp peaks in the dielectric constant as a function of the temperature in the BTNNO samples. Therefore, the paraelectric to ferroelectric transition temperature (T_C) is determined according to temperature dependent dielectric constant. The phase transition temperatures T_C are independent of applied frequency in all BTNNO ceramics which indicating that there is no glassy behavior and the presence of a long-range order state. The peaks in the dielectric constant are broadened with increasing x, which indicating the presence of disordered dipoles. It is clear that the phase transition temperature (T_C) moves towards the low temperature with the dopant concentration increasing, as shown in Fig. 2(f). The T_C of these components of the BTNNO ceramics decreases at approximately linear with the concentration. The crystalline structure changes from tetragonal phase to cubic phase with increasing dopant concentration, which is consistent with structural transformation indicated by X-ray diffraction data. It is found that the T_C of BTNNO samples with low dopant concentrations ($x < 0.06$) is higher than 300 K, which means that it can maintain well ferroelectricity at room temperature.

In order to examine the ferroelectricity for samples, P-E hysteresis loops with frequency at 100 Hz have been obtained, as depicted in Fig. 3. The applied field of each ceramics is 25 kV/cm. All ceramic samples show relatively full ferroelectric hysteresis loops. The pure BTO sample shows a well-saturated typical hysteresis loop and the hysteresis loops of these doped samples with increasing Ni-Nb concentration tend to be slimmer and narrower, which means that ferroelectricity of these doped samples is decrease. This behavior can be attributed to the phase transition tendency from tetragonal phase favoring ferroelectricity to cubic phase suppressing ferroelectricity, which weakened the electric polarization at room temperature. Compared with the tetragonal phase, the displacement of Ti^{4+} in the cubic phase is suppressed, which leads to a weakened macroscopic polarization[22]. As depicted in the Fig. 3(b), saturation polarization (P_m), remnant polarization (P_r) and coercive field (E_c) generally decrease with the increase of dopant concentration. The reduction in ferroelectric polarization is not as sharply as that of the single-doped samples. The co-doping strategy can slow down the rapid decrease in ferroelectricity because the incorporation of Nb^{5+} ions with its $4d^0$ configuration supporting ferroelectricity of samples plays a key role[23]. Thus, Ni-Nb co-doping can take advantage Nb doping and solve the problem of the Ni single-doping.

Figure 4 shows the M-H hysteresis loops of the BTNNO ceramics measured at room temperature. It is showed that the BTO ceramic is intrinsic diamagnetic and the BTNNO with $x = 0.02$ and 0.04 are combined by diamagnetic and ferromagnetic parts as shown in Fig. 4 (a). With the increase doping concentration, the plot of M-H shows that the samples have the S-type hysteresis loop obviously as $x \geq 0.06$ in Fig. 4(b), indicating the existence of ferromagnetic behavior obviously at room temperature. For clearly highlighting the contribution of the ferromagnetic part of samples of the S-type hysteresis loop showing apparent ferromagnetic, the M-H hysteresis loops subtracting linear part associated with the diamagnetism or paramagnetism are re-graphed as Fig. 4(c). It appears that the ferromagnetism increases with increasing x from 0.06 to 0.8, and further increase in dopant concentration will reduce ferromagnetism for $x = 0.1$. The F-center exchange (FCE) mechanism proposed by Coey *et al.* may be more reasonable to explain the formation of ferromagnetism in the doped BTO ceramics[24, 25]. BTNNO samples contain the oxygen vacancies that are to maintain charge neutrality when a Ti^{4+} ion is substituted in Ni^{2+} and Nb^{5+} ion. Therefore, oxygen vacancies increase with the doping concentration increasing. In BTNNO samples, the formation of an F center is due to the oxygen vacancies capture electrons. The FCE mechanism is that two Ni^{2+} ions interact with each other through oxygen vacancies: Ni^{2+} - $V_O{}^{2-}$- Ni^{2+}, where $V_O{}^{2-}$ denotes the oxygen vacancies. The bound electron occupying an orbital in the oxygen vacancy overlaps the d shells of neighboring magnetic ions Ni^{2+}. A ferromagnetic exchange interaction between two Ni^{2+} ions and an electron in oxygen vacancy may happen. Through ferromagnetic long-range exchange interaction, the magnetic moments of all Ni^{2+} ions become the same direction. Therefore, the formation of the F-center is usually the cause of ferromagnetism in BTNNO samples. Noticeably, the magnetization is reduced at a higher magnetic field at $x = 0.08$ doping, which indicates diamagnetism. This may be due to the suppression of the exchange interaction energy at the higher magnetic fields[26, 27]. The M-H hysteresis loops at high field show a linear relationship at $x = 0.1$ doping, which indicates that there is some paramagnetic phenomenon. The existence of some Ni^{2+} ions which do not ferromagnetically couple with the oxygen vacancies results in paramagnetic behavior[26]. The Ni^{2+} ions will approach each other with the increasing dopant concentration, which means that some Ni^{2+} ions are closest to Ni^{2+} ions rather than oxygen vacancies. However, the superexchange interactions between these adjacent Ni^{2+} ions are antiferromagnetic. Hence, the doping of Ni^{2+} ions at high concentration levels will suppress ferromagnetic coupling, resulting in a decrease in ferromagnetism.

Figure 5 shows the optical band gap energies of BTNNO ceramics. The optical band gap (E_g) is deduced via allowed direct inter-band transition between conduction and valence bands by Tauc's relation[28]: $(ahv)^2 = A(hv-E_g)$where α is the absorption coefficient, hv is the photon energy, A is a constant, and E_g is the optical band gap. As shown in Fig. 5, the Eg values can be attained from tangent lines in the curves of $(\alpha hv)^2$ versus hv. The value of the optical band gap is an intercept of $(\alpha hv)^2$ plot with the photon energy hv. It can be seen clearly that the band gap of the BTNNO samples is obviously reduced through the strategy of co-doping. The optical band gaps for BTNNO are 4.22, 3.61, 3.64, 3.69, 3.6 and 3.51 eV for x = 0, 0.02, 0.04, 0.06, 0.08 and 0.1, respectively. As showed in Fig. 5, the band gaps decrease from 4.22 eV in pure BTO to 3.51 eV in the x = 0.1 Ni-Nb substituted composition. Especially, it is found that the band gaps of our samples are relatively large. This may be due to the different fabrication conditions. It is well known that the bandgap value of BTO depends on the Ti 3d and O 2p states while Ba has no effect on the formation mechanism of the band gap in the BTO ceramics[29, 30]. The O 2p states result in the valence band maximum and the Ti 3d states contribute to the conduction band minimum in the BTO. The Nb 4d states are located above the conduction band[31]. Therefore, The Nb 4d states have no effect on the band gap of BTNNO ceramics. The 3d orbital of Ni^{2+} is split into e_g orbitals and t_{2g} orbitals under the influence of octahedral crystal field[32]. Further, the difference on Ni–O and Nb–O bond lengths caused by the off-centering displacement of the ions at B sites lead to the distortion of the octahedral. Then, the e_g states evolve into a low energy d_{z^2} state and a high energy $d_{x^2-y^2}$ state, and t_{2g} states transform into a high energy d_{xy} state and two low energy d_{zx} and d_{yz} states[30]. The formation a relatively narrow bandgap is mainly due to the inter-band transition from the d_{z^2} state to the $d_{x^2-y^2}$ state[30].

4. Conclusion

In summary, ceramics of x = 0, 0.02, 0.04, 0.06, 0.08 and 0.1 Ni-Nb co-doped BTO ceramics were successfully synthesized through conventional solid-state sintering methods. Structural measurement exhibits the BTNNO ceramics undergo a structural transition from tetragonal phase to cubic phase with increasing dopant concentration by the X-ray diffraction analysis. The P-E curves of BTNNO samples show that the ferroelectricity is weakened slowly after Ni-Nb co-doping, which is consistent with the X-ray diffraction results. Through the incorporation of the magnetic element Ni, the magnetic properties of the BTNNO ceramics gradually change from diamagnetism to ferromagnetism with increasing x. In addition, the optical analysis of BTNNO samples suggests that the decrease of band gaps can be attributed to the 3d orbitals splitting of Ni^{2+} ions. Our research of BTNNO ceramics provides useful information which implies that the BTNNO ceramics may have potential application as multiferroic materials in the future.

Declarations

Acknowledgements

This work is supported by the National Key Research and Development Program of China (2017YFA0303403), the National Natural Science Foundation of China (61674058, 61574058).

References

1. S. Dong, J.M. Liu, S.W. Cheong, Z. Ren, Adv. Phys. **64**, 519–626 (2015)
2. W. Eerenstein, N.D. Mathur, J.F. Scott, Nature **442**, 759–762 (2006)
3. T.G.T. Kimura, H. Shintani, K. Ishizaka, T. Arima, Y. Tokura, Nature **426**, 55–58 (2003)
4. M. Corasaniti, P. Barone, A. Nucara, M. Ortolani, L. Baldassarre, R. Fittipaldi, V. Granata, L. Rocco, A. Vecchione, W.S. Mohamed, J. Lorenzana, P. Calvani, Phys. Rev. B **96**, 085115 (2017)
5. N.A. Benedek, C.J. Fennie, J. Phys. Chem. C **117**, 13339–13349 (2013)
6. N.A. Hill, J. Phys. Chem. B **104**, 6694–6709 (2000)
7. D.I. Khomskii, J. Magn. Magn. Mater. **306**, 1–8 (2006)
8. J.F. Scott, Science **315**, 954–959 (2007)
9. A. Rani, J. Kolte, P. Gopalan, Ceram. Int. **41**, 14057–14063 (2015)
10. S. Sahoo, P.K. Mahapatra, R.N.P. Choudhary, P. Alagarsamy, Mater. Res. Express **5**, 016101 (2018)
11. N. Hiroyuki, H. Katayama-Yoshida, Jpn. J. Appl. Phys. **40**, L1355–L1358 (2001)
12. J.S. Lee, Z.G. Khim, Y.D. Park, D.P. Norton, J.D. Budai, L.A. Boatner, S.J. Pearton, R.G. Wilson, Electrochem. Solid-State Lett. **6**, J1–J3 (2003)
13. L. Zhou, Y. Zhang, S. Li, Q. Lian, J. Yang, W. Bai, X. Tang, J. Mater. Sci.-Mater. Electron. **31**, 14487–14493 (2020)
14. M. Zhou, J. Zhang, L. Ji, Y. Wang, J. Wang, F. Yu, Ceram. Int. **40**, 853–857 (2014)
15. Y.H. Lin, J. Yuan, S. Zhang, Y. Zhang, J. Liu, Y. Wang, C.-W. Nan, Appl. Phys. Lett. **95**, 033105 (2009)
16. S.F. Wang, Y.C. Wu, Y.C. Hsu, J.P. Chu, C.H. Wu, Jpn. J. Appl. Phys. **46**, 2978–2983 (2007)
17. S. Das, S. Ghara, P. Mahadevan, A. Sundaresan, J. Gopalakrishnan, D.D. Sarma, ACS Energy Lett. 3, (2018)
18. N.V. Dang, N.T. Dung, P.T. Phong, I.-J. Lee, Phys. B **457**, 103–107 (2015)
19. R. Wäsche, W. Denner, H. Schulz, Mater. Res. Bull. **16**, 497–500 (1981)
20. S.K. Das, R.N. Mishra, B.K. Roul, Solid State Commun. **191**, 19–24 (2014)
21. B. Zhong, Z. Long, C. Yang, Y. Li, X. Wei, Ceram. Int. **46**, 20565–20569 (2020)
22. Y. Shuai, S. Zhou, D. Bürger, H. Reuther, I. Skorupa, V. John, M. Helm, H. Schmidt, J. Appl. Phys. **109**, 084105 (2011)
23. N. Masó, H. Beltrán, E. Cordoncillo, A.A. Flores, P. Escribano, D.C. Sinclair, A.R. West, J. Mater. Chem. **16**, 3114–3119 (2006)
24. J.M.D. Coey, A.P. Douvalis, C.B. Fitzgerald, M. Venkatesan, Appl. Phys. Lett. **84**, 1332–1334 (2004)
25. J.M.D. Coey, M. Venkatesan, C.B. Fitzgerald, Nat. Mater. **4**, 173–179 (2005)

26. M. Arshad, W. Khan, M. Abushad, M. Nadeem, S. Husain, A. Ansari, V.K. Chakradhary, Ceram. Int. **46**, 27336–27351 (2020)
27. P. Sharma, P. Kumar, R.S. Kundu, N. Ahlawat, R. Punia, Ceram. Int. **42**, 12167–12171 (2016)
28. M.S. Mostari, M.J. Haque, S. Rahman Ankur, M.A. Matin, A. Habib, Mater. Res. Express **7**, 066302 (2020)
29. B. Weng, Z. Xiao, W. Meng, C.R. Grice, T. Poudel, X. Deng, Y. Yan, Adv. Energy Mater. **7**, 1602260 (2017)
30. D. Zheng, H. Deng, S. Si, Y. Pan, Q. Zhang, Y. Guo, P. Yang, J. Chu, Ceram. Int. **46**, 6073–6078 (2020)
31. F. Yang, L. Yang, C. Ai, P. Xie, S. Lin, C.Z. Wang, X. Lu, Nanomaterials **8**, 455 (2018)
32. J. Yin, Z. Zou, J. Ye, J. Phys. Chem. B **107**, 4936–4941 (2003)

Figures

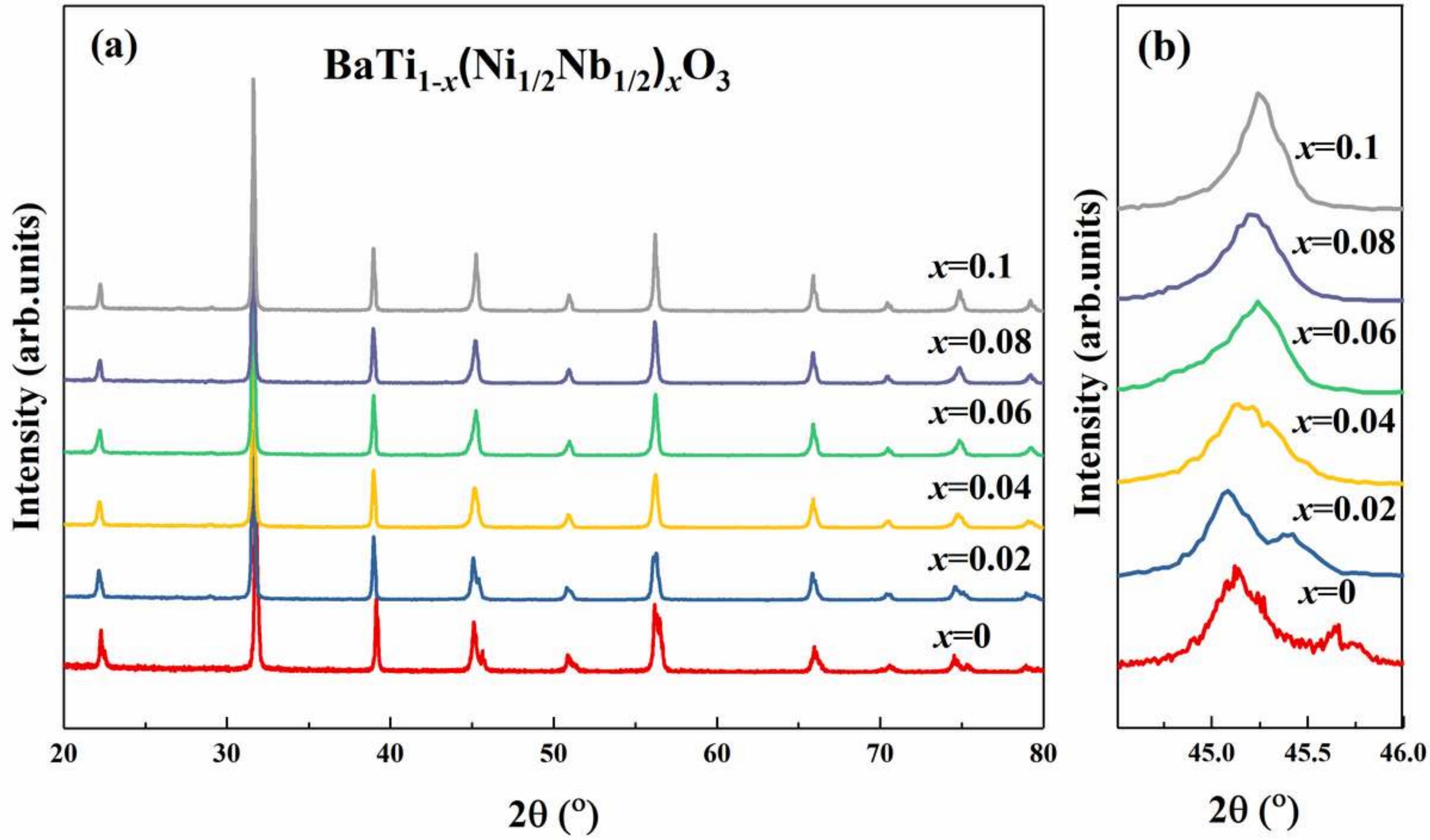

Figure 1

(a) XRD patterns of BaTi1-x(Ni1/2Nb1/2)xO3 ceramics. (b) Magnified patterns around 2θ =45o.

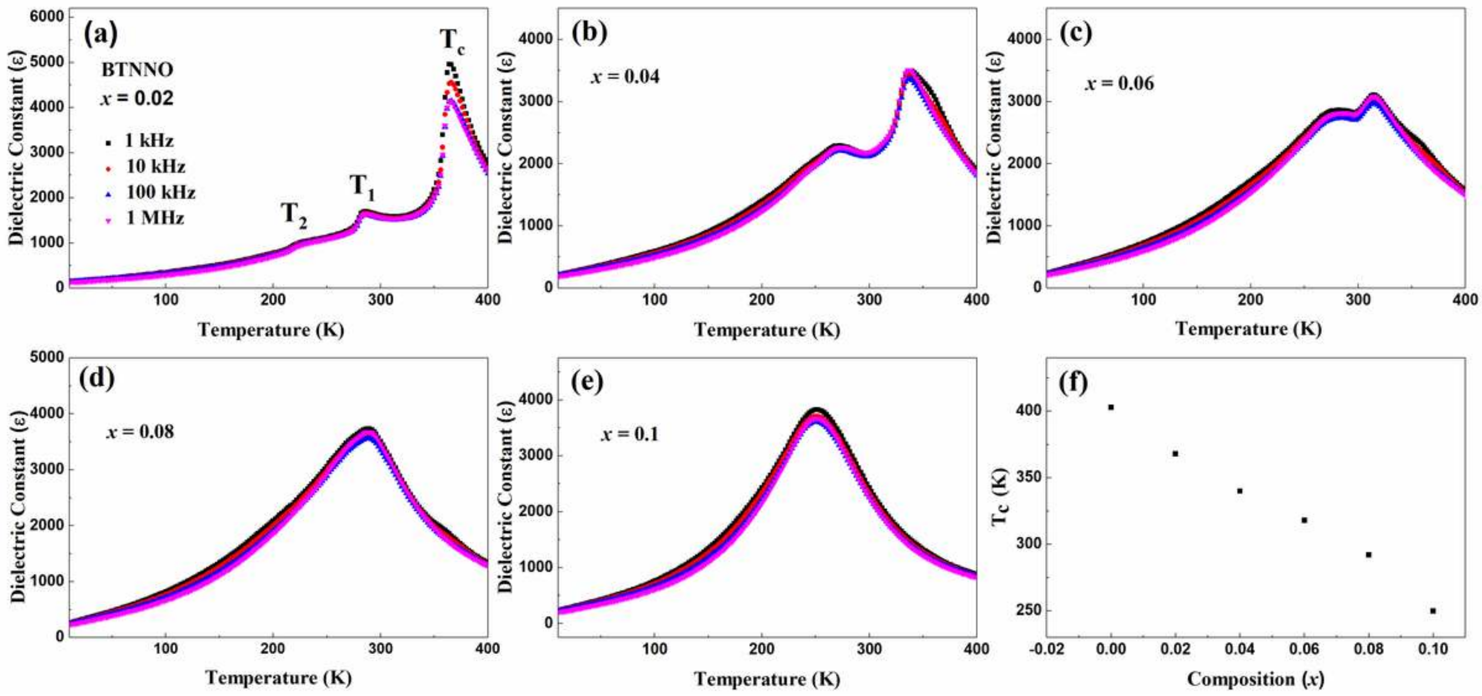

Figure 2

(a-e) Temperature dependence of dielectric constant of BaTi1-x(Ni1/2Nb1/2)xO3 samples measured at the range of 1 kHz to 1 MHz; (f) Curie temperature as a function of composition x.

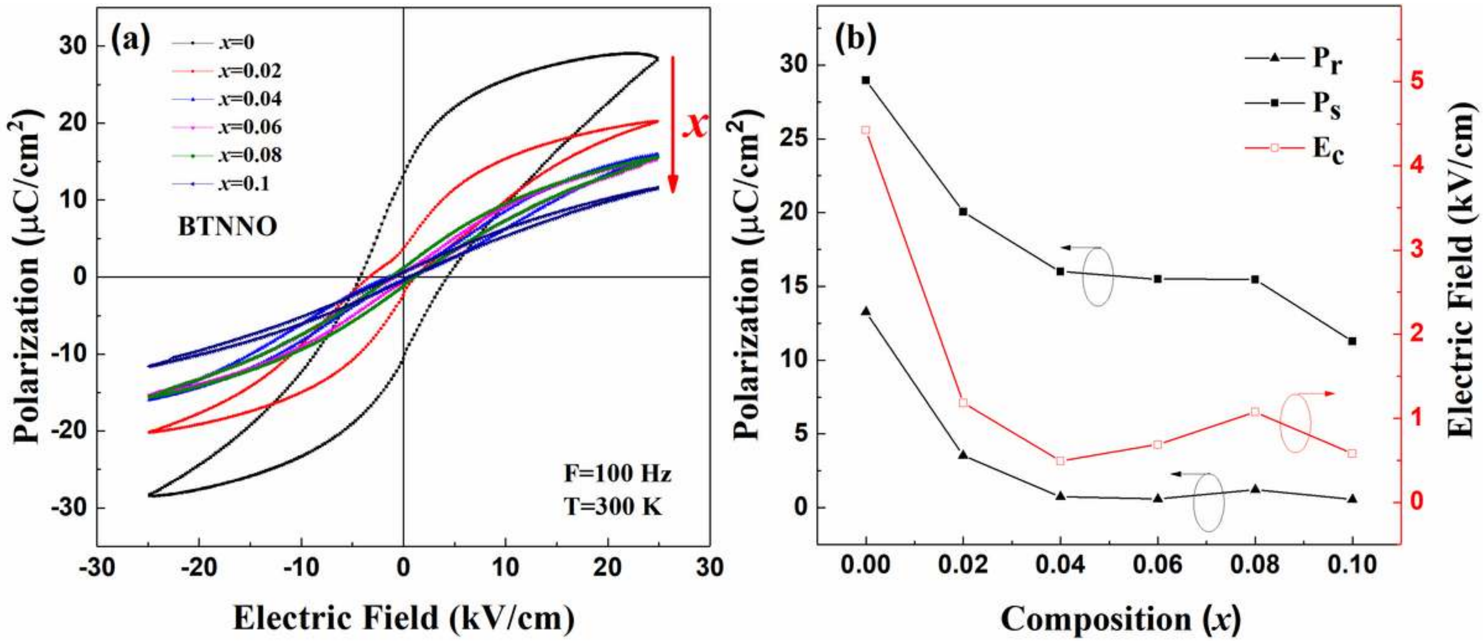

Figure 3

(a)P-E hysteresis loops of doped BTNNO samples at room temperature under an electric field of 25 kV/cm; (b) detail of P-E hysteresis loops.

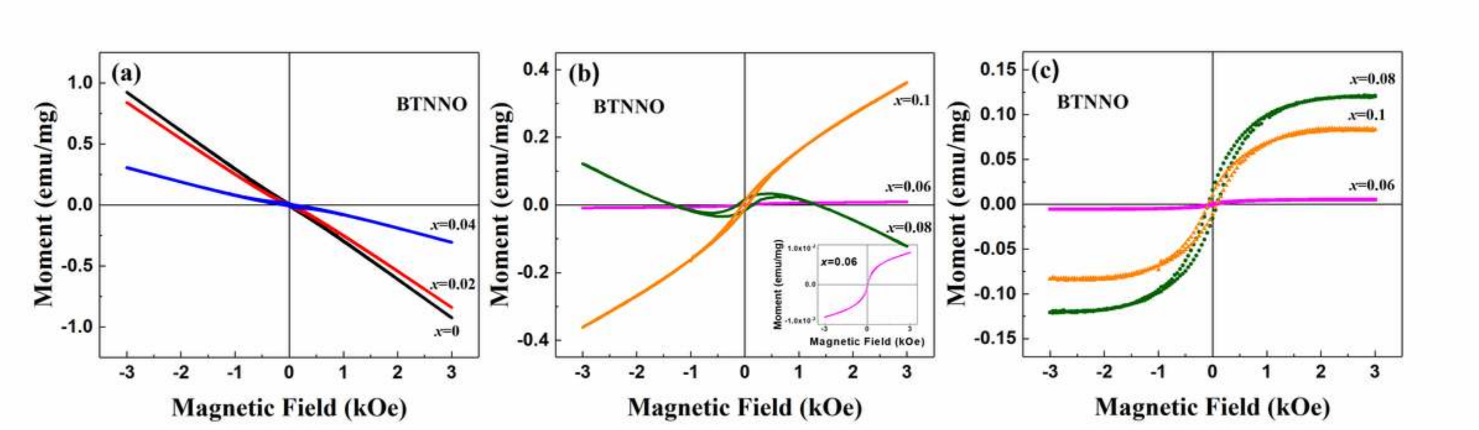

Figure 4

M-H hysteresis loops of the BaTi1-x(Ni1/2Nb1/2)xO3 ceramics at 300 K (a) x=0-0.04; (b) x=0.06-0.1 and the inset is an enlarged view of the x=0.06 components. (c) M-H hysteresis loops after subtracting the paramagnetic or diamagnetic contributions of BTNNO x = 0.06-0.1.

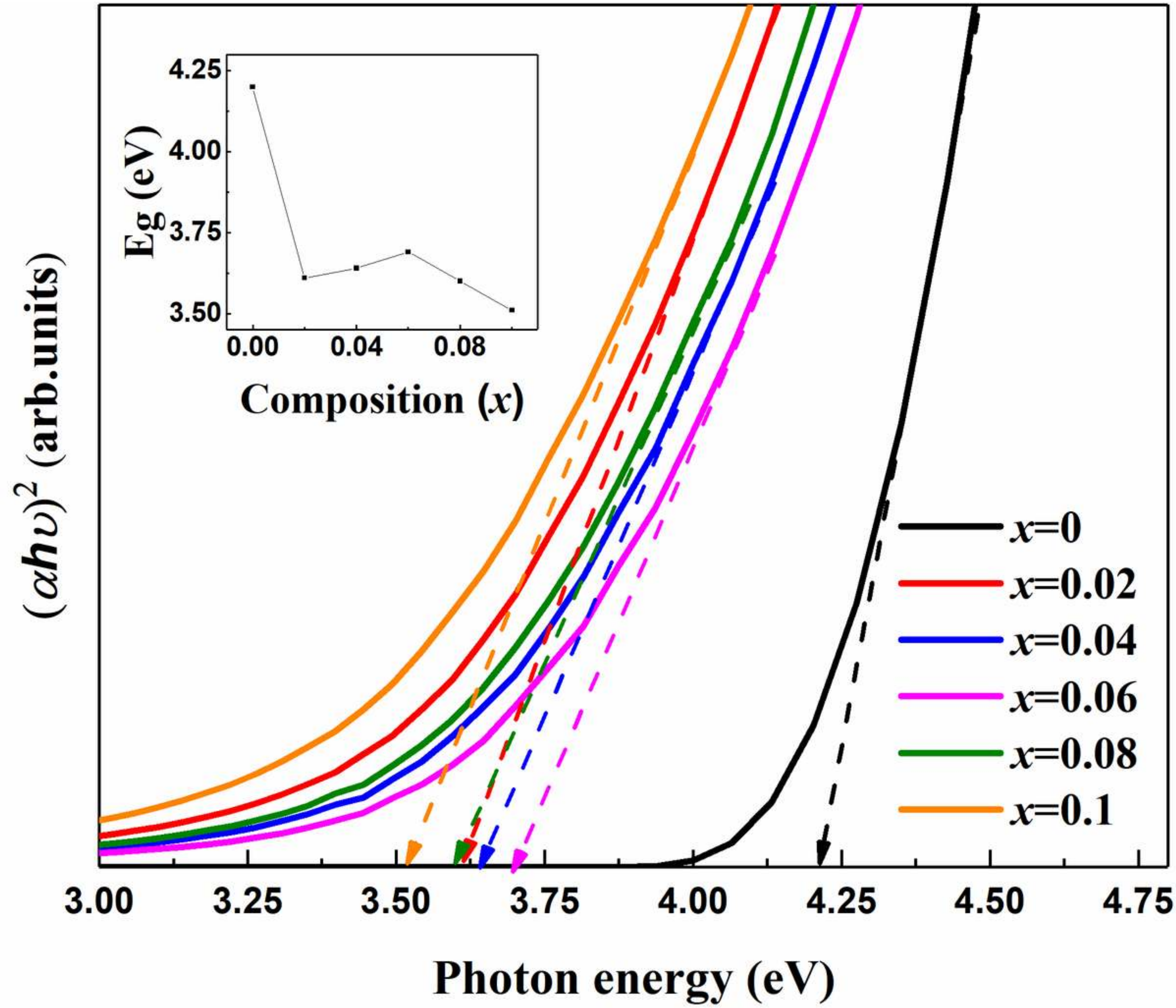

Figure 5

Plots of (ahv)2 vs the photon energy for the estimation of optical band gap energies from the BTNNO (0≤x≤0.1). The inset shows the relationship between optical band gap and composition.